REPORT DOCUMENTATION PAGE

Form Approved OMB No. 0704-0188

1. REPORT DATE *(DD-MM-YYYY)*	2. REPORT TYPE	3. DATES COVERED *(From - To)*
30-Sep-2008	REPRINT	

4. TITLE AND SUBTITLE
WAVE PROPAGATION FROM COMPLEX 3D SOURCES USING THE REPRESENTATION THEOREM

5a. CONTRACT NUMBER
FA8718-08-C-0010

5b. GRANT NUMBER

5c. PROGRAM ELEMENT NUMBER
62601F

6. AUTHOR(S)
Jeffry L. Stevens and Heming Xu

5d. PROJECT NUMBER
1010

5e. TASK NUMBER
SM

5f. WORK UNIT NUMBER
A1

7. PERFORMING ORGANIZATION NAME(S) AND ADDRESS(ES)

Science Applications International Corporation
10260 Campus Point Drive
San Diego, CA 92121-1152

8. PERFORMING ORGANIZATION REPORT NUMBER

9. SPONSORING / MONITORING AGENCY NAME(S) AND ADDRESS(ES)
Air Force Research Laboratory
29 Randolph Road
Hanscom AFB, MA 01731-3010

10. SPONSOR/MONITOR'S ACRONYM(S)
AFRL/RVBYE

11. SPONSOR/MONITOR'S REPORT NUMBER(S)
AFRL-RV-HA-TR-2008-1099

12. DISTRIBUTION / AVAILABILITY STATEMENT
Approved for Public Release; Distribution Unlimited.

13. SUPPLEMENTARY NOTES
Reprinted from: Proceedings of the 30th Monitoring Research Review – Ground-Based Nuclear Explosion Monitoring Technologies, 23 – 25 September 2008, Portsmouth, VA, Volume I pp 682 - 691.

14. ABSTRACT
In spite of extensive prior research on the generation of seismic waves by underground nuclear explosions, it is still not possible to provide a complete explanation for the observed wavefields, particularly at regional distances. Spherically symmetric explosion models embedded in layered elastic media effectively model the P phases generated by explosions and the major characteristics of some reflected and transmitted phases. Nonlinear axisymmetric finite difference calculations of explosions, including gravity and the effect of the free surface, can model a more realistic explosion source that directly generated shear waves. These models explain more characteristics of explosion-generated seismic waves, including some aspects of regional shear phases. However, it is clear that linear and nonlinear near-source 3D effects are important in many cases. SH waves are commonly observed within a few kilometers of explosions, too close to have been generated by (simple) conversion of vertical and radial components, and often larger than those components. Furthermore, it has not been established what impact 3D effects have on discriminants and on explosion yield estimates. It is important, therefore, to be able to model and understand how 3D source and source region heterogeneity affect the seismic wavefield and what impact this has on parameters used for nuclear monitoring. In this new project, we are implementing a technique that allows us to propagate the results of near-source 3D finite difference calculations to regional and teleseismic distances, and to use the results to investigate the impact of 3D near-source effects on regional and teleseismic phases, focusing in particular on the generation of SH phases by explosion sources. Our approach is to perform 3D explosion source region calculations, and then to propagate the wavefield to local, regional and teleseismic distances using layered earth Green's functions. We are interested in near-source heterogeneities in both the nonlinear and linear regimes, and therefore require both nonlinear and linear 3D codes to model the source region. In previous projects, we have used two nonlinear codes, STELLAR and CRAM, and the 3D linear elastic code TRES3D. STELLAR is an Eulerian 2D and 3D code well suited to performing near-source calculations, and CRAM is a 2D axisymmetric Lagrangian code that is capable of modeling the transition zone between the vaporized explosion cavity and linear elastic region, including the effects of gravity and the free surface. As part of this project, we are developing a 3D Lagrangian code with the material models and capabilities of CRAM, and we are developing the interface code to propagate 3D near source waveforms to regional and teleseismic distances using full waveform, modal and far-field body wave Green's functions. The first part of this project has focused on the development of these numerical tools that will be used throughout the project. Our plans are to perform calculations for realistic near-source 3D heterogeneity in the nonlinear region; to propagate these calculations to local, regional, and teleseismic distances; and to compare results with explosion-generated waveforms.

15. SUBJECT TERMS
Synthetic seismograms, Seismic sources, 3D models

16. SECURITY CLASSIFICATION OF:			17. LIMITATION OF ABSTRACT	18. NUMBER OF PAGES	19a. NAME OF RESPONSIBLE PERSON
a. REPORT	b. ABSTRACT	c. THIS PAGE			Robert J. Raistrick
UNCLAS	UNCLAS	UNCLAS	SAR	10	19b. TELEPHONE NUMBER *(include area code)* 781-377-3726

Standard Form 298 (Rev. 8-98)
Prescribed by ANSI Std. 239.18

WAVE PROPAGATION FROM COMPLEX 3D SOURCES USING THE REPRESENTATION THEOREM

Jeffry L. Stevens and Heming Xu

Science Applications International Corporation

Sponsored by Air Force Research Laboratory

Contract No. FA8718-08-C-0010
Proposal No. BAA08-57

ABSTRACT

In spite of extensive prior research on the generation of seismic waves by underground nuclear explosions, it is still not possible to provide a complete explanation for the observed wavefields, particularly at regional distances. Spherically symmetric explosion models embedded in layered elastic media effectively model the P phases generated by explosions and the major characteristics of some reflected and transmitted phases. Nonlinear axisymmetric finite difference calculations of explosions, including gravity and the effect of the free surface, can model a more realistic explosion source that directly generated shear waves. These models explain more characteristics of explosion-generated seismic waves, including some aspects of regional shear phases. However, it is clear that linear and nonlinear near-source 3D effects are important in many cases. SH waves are commonly observed within a few kilometers of explosions, too close to have been generated by (simple) conversion of vertical and radial components, and often larger than those components. Furthermore, it has not been established what impact 3D effects have on discriminants and on explosion yield estimates. It is important, therefore, to be able to model and understand how 3D source and source region heterogeneity affect the seismic wavefield and what impact this has on parameters used for nuclear monitoring.

In this new project, we are implementing a technique that allows us to propagate the results of near-source 3D finite difference calculations to regional and teleseismic distances, and to use the results to investigate the impact of 3D near-source effects on regional and teleseismic phases, focusing in particular on the generation of SH phases by explosion sources. Our approach is to perform 3D explosion source region calculations, and then to propagate the wavefield to local, regional and teleseismic distances using layered earth Green's functions. We are interested in near-source heterogeneities in both the nonlinear and linear regimes, and therefore require both nonlinear and linear 3D codes to model the source region. In previous projects, we have used two nonlinear codes, STELLAR and CRAM, and the 3D linear elastic code TRES3D. STELLAR is an Eulerian 2D and 3D code well suited to performing near-source calculations, and CRAM is a 2D axisymmetric Lagrangian code that is capable of modeling the transition zone between the vaporized explosion cavity and linear elastic region, including the effects of gravity and the free surface. As part of this project, we are developing a 3D Lagrangian code with the material models and capabilities of CRAM, and we are developing the interface code to propagate 3D near source waveforms to regional and teleseismic distances using full waveform, modal and far-field body wave Green's functions.

The first part of this project has focused on the development of these numerical tools that will be used throughout the project. Our plans are to perform calculations for realistic near-source 3D heterogeneity in the nonlinear region; to propagate these calculations to local, regional, and teleseismic distances; and to compare results with explosion-generated waveforms.

OBJECTIVES

The objective of this project is to investigate the generation of complex seismic waves by explosions in media with 3D heterogeneity using a method based on the exact representation theorem for propagating complex 3D-source calculations to local, regional, and teleseismic distances at which they are observed.

RESEARCH ACCOMPLISHED

Introduction

Source physics, near-source scattering, and propagation effects are all important to understanding seismic phases used in nuclear monitoring. Significant bodies of literature exist that address each subject individually. In addition to extending our understanding of source physics and near-source scattering to include the effects of realistic 3D heterogeneity, this new project links the progression of energy from its generation by the source, through the near-source region, and on into its partitioning among local, regional, and teleseismic phases. Distinguishing the far-field P and S waves enables us to quantify the effects of 3D structure on both P- and S-wave generation. Complete regional waveforms show how this energy is partitioned among the distinct phases important to event detection, identification, and magnitude estimation. How energy is distributed among surface wave modes determines Lg amplitudes and Rg amplitudes, including near-source conversions between these phases. Modal excitation of Lg as well as Rg has a significant depth dependence that is often neglected in nuclear monitoring studies (Baker et al., 2004), and these amplitudes can be disrupted further by near source effects and source region structure. This can either degrade or improve discrimination capability, depending on how well it is understood.

As an example of anomalous (but almost universally observed) SH waves from explosions, we present data from the Soviet Peaceful Nuclear Explosions (PNE) Quartz3 and Quartz4 (Figure 1, left). Figure 1 (right) shows an example of strong tangential component S waves from the Quartz 3 PNE. This 8.5-kiloton explosion was overburied by a factor of 3 relative to normal scaled depth, at a depth of 759 meters. This event should therefore be a good approximation to the ideal point, spherical explosion source. Nevertheless, it generated strong SH waves. Figure 2 shows an image of the source location. As indicated by the meandering river, the site is quite flat, so topography would be expected to have little effect on the seismic waves. Tangential component S at large distances would not be surprising, as the components gradually homogenize with distance; however, in this case the S waves exist strongly across the entire section, suggesting that they leave the source region as SH waves, rather than being rotated into that orientation by structure during propagation.

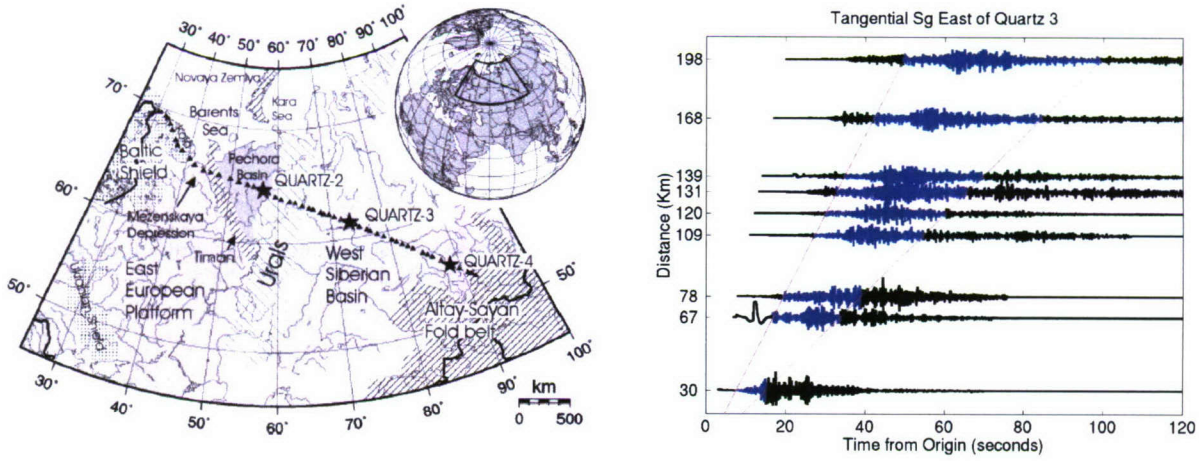

Figure 1. Layout of stations from the Quartz3 and Quartz4 PNE (left) and tangential component S waves from Quartz3 (right). The blue part of the time series and the red lines delimit 4 to 2 km/s. Strong SH waves exist over the entire section.

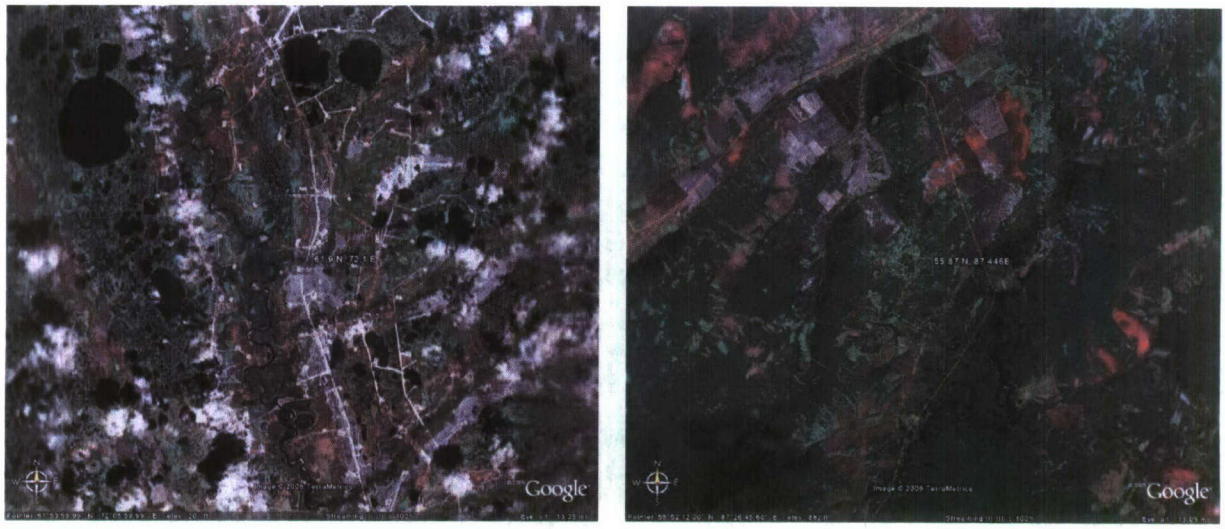

Figure 2. Quartz3 location (left) and Quartz4 location (right). Each image is 24 km by 20 km. The explosion location is in the center of each figure. Both sites are quite flat. Granite can be seen at the surface at the Quartz 4 location.

Quartz4 was a 10-kt explosion at slightly shallower depth (557 m) than Quartz3 but still overburied by a factor of 2. The explosion is in granite, and granite can be seen at the surface near the explosion site in Figure 2. Again, there is little apparent topography. Kitov (1997) states that "Geological structure for Quartz4 may be characterized as a homogeneous half-space covered by a thin (10 to 15 m) layer of soil." Figure 3 shows the three components of the Quartz4 seismograms at a station 31 km to the east. There is a strong SH wave on the tangential component and no obvious trace of it on either the vertical or radial component. Very similar observations were made for the deep U.S. explosion Rulison (Figure 3, right).

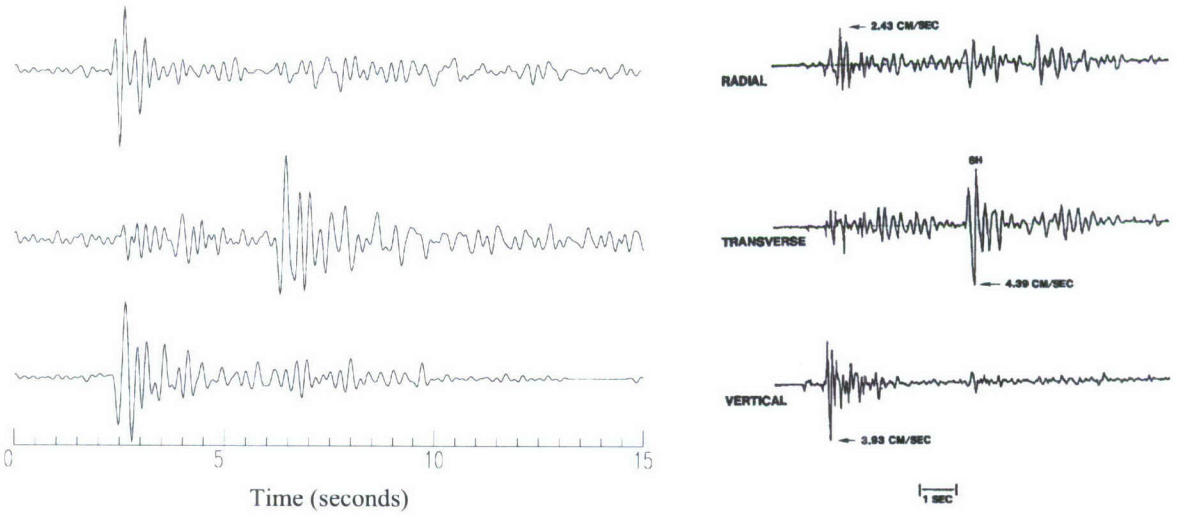

Figure 3. Left: Radial (top), transverse (center), and vertical (bottom) seismograms from Quartz4 observed 31 km east of the explosion. Data have been bandpass filtered between 1 and 5 Hz. There is a strong SH phase on the tangential that does not exist on the radial or vertical components. Right: Similar figure showing seismograms at a distance of 23 km from the deep U.S. explosion Rulison (from Murphy and Archambeau, 1986).

These examples (and many others) point to the need to understand 3D source effects. While it is not surprising to see SH waves from any single event, what is surprising is that they are always present and, at regional distances, scale with yield about as well as P waves. That is, while there are many mechanisms such as near-source scattering,

tectonic release, etc., that can generate SH waves, all of these effects should be highly variable from one event to the next. To address this question, we need to look at the types of 3D source effects that can exist, the range of variability that would be expected from them, and whether the predictions are consistent with observations.

Source Region Calculations and Propagation Using the Representation Theorem

Our approach is to perform 3D explosion source region calculations and then to propagate the wavefield to local, regional, and teleseismic distances, using layered-earth Green's functions. We are interested in near-source heterogeneities in both the nonlinear and linear regimes and therefore require both nonlinear and linear 3D codes to model the source region. In previous projects, we have used two nonlinear codes, STELLAR and CRAM, which are described briefly in Table 1 (we have also used the 1D nonlinear code SKIPPER, which is a spherically symmetric version of CRAM), and the 2D and 3D linear elastic code TRES3D.

Table 1. Numerical simulation tools to be used in this project

Numerical Simulation Tools	
STELLAR	Eulerian finite-difference code. Used to simulate the early time history of the explosion shock. It handles material strength correctly, which is difficult for an Eulerian code. Uses a second-order accurate Riemann solver scheme. 1D, 2D planar and axisymmetric, and 3D.
CRAM	Lagrangian nonlinear finite difference code. Has been used extensively for axisymmetric explosion calculations. A 3D version of the code is being developed in this project.
TRES3D	Elastic finite difference code. 2D planar and axisymmetric, and 3D.
Elastodynamic Representation Theorem	The time-dependent displacements and stresses from 3D source region calculations are saved on a monitoring surface located outside the region of nonlinear response and/or 3D heterogeneity. A numerical implementation of the representation integral is then used to compute the corresponding far-field seismic radiation.

In past projects, we have used these codes in the following ways:

1. Axisymmetric CRAM was used together with the representation theorem to propagate the results of nonlinear axisymmetric finite-difference calculations to regional and teleseismic distances (Day et al., 1987; Stevens et al., 1991; Stevens et al., 2004).
2. Axisymmetric STELLAR was used to calculate the early stages of an explosion. The solution at an appropriate time was overlaid onto CRAM to be propagated out to the linear, elastic region. The representation theorem was used to propagate the waveform to regional and teleseismic distances (Rimer et al., 1994). A similar technique was used to overlay results from the LANL code SOIL onto CRAM and propagate the results (Davis et al., 1992).
3. 3D STELLAR was used to calculate near-field waveforms from explosions in rectangular cavities (Stevens et al, 2006).
4. TRES3D was used to calculate the scattering from explosions in a region with 3D heterogeneity and topography (Stevens et al., 2004).

In the current project, we are doing the following: (1) using STELLAR to perform very near source nonlinear 3D calculations and TRES3D to perform linear elastic near-source and source region 3D calculations, (2) developing a 3D version of CRAM to model explosions from the source out through the very important nonlinear-to-linear transition region, and (3) completing the implementation of the elastodynamic representation theorem for full waveforms, modes, and body waves.

The technique for propagating numerical calculations using the representation theorem is to save displacements and stresses on a monitoring surface surrounding the nonlinear and/or heterogeneous region of the calculation and then to convolve these with a Green's function appropriate for the external region (Stevens et al., 1991). In the cases that we have done previously, 2D axisymmetric nonlinear finite-difference calculations were performed to model the nuclear explosion, and the stresses and displacements from the calculation were saved on a cylindrical surface in the elastic region outside the region of complex nonlinear behavior. We then invoked the representation theorem and integrated the stresses and displacements with an axisymmetric Green's function to calculate the displacement at any

point outside the calculation. We performed such calculations in 2D, using Green's functions for far-field body waves, for modes, and for full regional waveforms using wavenumber integration. The equations for the Green's functions for surface waves are given by Bache et al. (1982). The Green's functions for the complete seismograms are computed using a ring load source, from an algorithm based on the work of Luco and Apsel (1983) and Apsel and Luco (1983). The Green's functions for body waves are generated by a procedure similar to that described by Bache and Harkrider (1976), using a saddle point approximation to calculate a far-field plane wave for a given takeoff angle from a source in a plane-layered medium. Our objective in using multiple types of Green's functions is to gain as much insight as possible into the nature of the seismic wavefield generated by the source. An important part of the current project is to adapt these techniques to propagate seismic waves from 3D source calculations. Although any closed surface can be used for representation theorem integration, we use a cylindrical surface for axisymmetric problems and a rectangular surface for 3D problems.

3D Implementation of the Representation Theorem

The key to extending the axisymmetric representation theorem discussed above to 3D is to recognize that while the deformation in the source region may be arbitrarily complex, if the structure can be approximated as a plane-layered medium outside of the source region, then the known Green's function for a plane-layered medium applies (this also assumes that we can neglect the interaction of any backscattered waves returning to the source region after leaving it). Note that the representation theorem is exact. That is, no matter how complex the 3D motion is on the source region boundary, it will be correctly propagated by the representation theorem. The following benchmark test demonstrates the performance of the method by comparing the results with equivalent finite difference calculations and wavenumber integration seismograms.

The representation theorem states that displacement at an observation point is made up of contributions due to body forces throughout the source volume, plus contributions due to the traction and displacement on the source volume surface (Aki and Richards, 1980). In the three-dimensional numerical finite difference calculations, we save displacements and stresses due to the seismic source on a monitoring surface on the boundary of a rectangle (5 planar surfaces, excluding the upper surface), and calculate Green's functions from each point on the monitoring surface to the receiver. Thus the synthetic seismogram at the receiver point X outside of the monitoring surface is obtained by integrating over the monitoring surface S_M

$$u_i = \iint_{S_M} \left\{ G_j^i(\xi; X) * T_j^M(\xi) - u_j^M(\xi) * S_{jk}^i(\xi; X) n_k \right\} dA \qquad (1)$$

in the frequency domain, where $G_j^i(\xi; X)$ and $S_{jk}^i(\xi; X)$ are the Green's function and the stress tensor on the monitoring surface due to a unit impulsive force at X in direction i, T_j^M is the traction on the monitoring surface due to the seismic source, u is the displacement on the monitoring surface, and n is the normal to the monitoring surface. The operator * denotes convolution, and the summation convention is assumed.

Equation 1 is applicable to any Green's function for the exterior model, and so we can use a full waveform Green's function, far-field body wave Green's function, and/or modal Green's function, as we have discussed earlier for axisymmetric problems. We have implemented this technique for full waveform seismograms, calculating the Green's functions using wavenumber integration. We plan to implement the technique for body waves and modes later in this project.

The synthetic seismograms are computed using the following steps:

1. Displacements and stresses are saved on the monitoring surface during the finite-difference calculations.
2. If necessary, the monitoring solutions are resampled onto a coarse grid, as permitted by the required resolution. If there is a symmetry boundary, the entire monitoring surface is constructed first.
3. The finite-difference solutions at each point on the monitoring surface are transformed into the frequency domain.
4. The displacement and stress Green's functions due to the three orthogonal forces at the receiver location are calculated for each location on the monitoring surface in the frequency domain (using reciprocity).
5. Equation (1) is used to obtain the solution at the receiver in the frequency domain.

6. The solution is transformed back to the time domain.

Figure 4 shows an example of a test of this technique. In this test case, full waveform synthetics are generated from a 3D elastic finite-difference calculation in two ways: (1) by using the representation theorem to propagate the waveforms outside of the source region and (2) by direct calculation using the same finite-difference code. The comparison is very good, which shows that the representation theorem technique is working correctly and that we can effectively use the representation theorem to extend the size of the finite-difference calculation to any desired range, provided that the earth can be modeled as a plane-layered structure at points outside the monitoring surface. The technique also requires that the material properties at the boundary of the calculation match the plane-layered structure. We have implemented the technique for full waveform seismograms and plan to do the same for modal seismograms and far-field body waves as part of this project. The reason for implementing the other Green's functions is that the modal decomposition allows us to look at the effects on individual modes, and the far-field body wave representation provides the clearest picture of the P and S waves generated by the source.

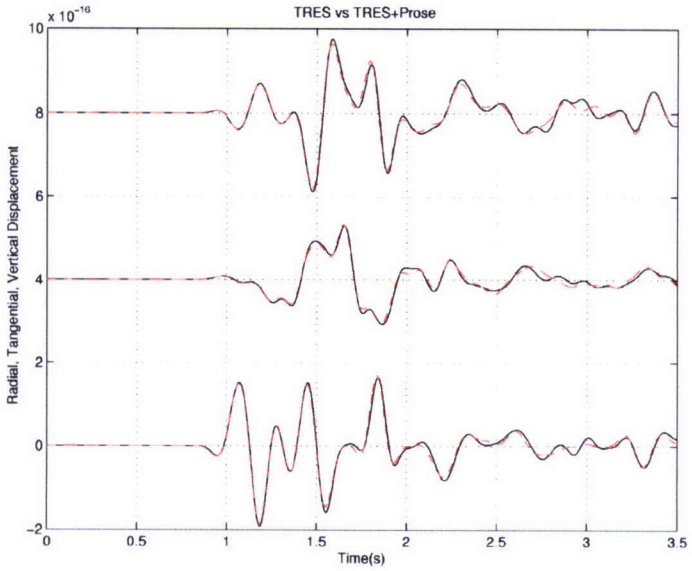

Figure 4. Comparison between solutions using the finite-difference method (solid lines) and the solutions using the representation theorem (dashed line) at a distance of 2561 m. The three curves from bottom to top are the radial, tangential, and vertical components.

The principal advantage of this approach is that it allows us to perform detailed calculations of the source region and then propagate the results to distances that would be impractical or impossible to include in the same numerical calculation. In addition to reducing cost and time, the hybrid method is also more accurate, as numerical dispersion increases with the size and duration of numerical calculations. A similar approach (in reverse) was used by Moczo et al. (1997) to calculate the effect of topography and near-surface structure on ground motion caused by a distant source. Wu et al. (2004, and earlier papers starting with Xie and Lay, 1994) used a similar concept by performing near-source finite-difference calculations followed by a calculation of slowness at large distances, which they then used to estimate the energy trapped in the crust versus lost to the mantle for different scattering scenarios. A significant advantage of the representation theorem approach described here is that we can also calculate waveforms at any location.

Development of a 3D Nonlinear Finite Element Code

A difficult task in this new project is development of a 3D nonlinear code with capabilities similar to our 2D axisymmetric finite-difference code CRAM. CRAM has a long history of successful calculation of explosions, and has well-tested material models. It also has the capability of including gravity and can model spall and other free-surface nonlinear interactions. For the current project, we are using a finite element code, as this is more easily adapted to complex 3D geometries. In particular, the cavity can be any shape, and the media can be nonlinear and heterogeneous.

We have implemented an explicit 3D Lagrangian finite-element algorithm that is capable of using multiple processors. All of the nonlinear material models from 2D CRAM have been implemented. The cavity is placed near the center of the grid and is enclosed by a spider grid that facilitates applying the pressure boundary condition and rezoning elements, as implemented in the 2D axisymmetric code, CRAM. Examples of the spider grid and outer grid are shown in Figure 5.

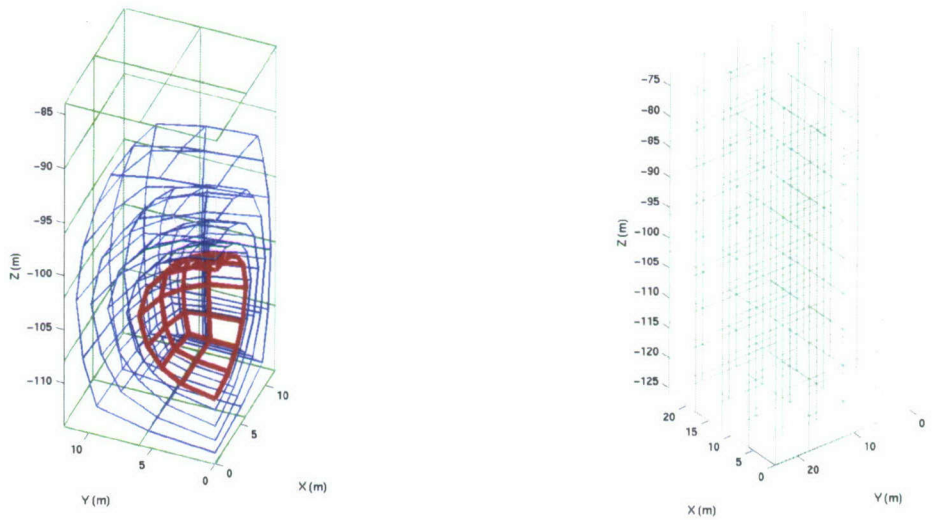

Figure 5. Left: Schematic of one quadrant of the spider grid. The red grid lines represent the cavity boundary, the blue lines represent the tangential grid lines inside the spider grid, and the green lines represent the interface between the spider grid and the outer Cartesian grid. Right: The outer Cartesian grid enclosing the spider grid (left).

In the numerical scheme, the wavefields in every element are computed, then the wavefields at each grid are computed by summing the contributions from each adjacent element (Ma and Liu, 2006). Since the one-point integration method is used for efficiency and flexibility, the resulting hourglass modes are damped, using both a viscous hourglass control scheme and a stiffness hourglass control scheme for large deformation. For grid stability due to strong shock-wave propagation, artificial viscosity is also necessary. Both linear and quadratic viscosity (extended from 2D CRAM) have been implemented.

Benchmark Tests

As a first benchmark test on the implementation of the finite element method, we calculate the dynamic response of a half-space to a pressure pulse applied to the wall of a spherical cavity with a 2-m radius buried 12 m deep in a linear elastic medium and compare this with the analytical results obtained using the point source theory of de Hoop (Jiang et al., 1994). The agreement is excellent and is the first step in validating the implementation of the finite-element algorithm (Figure 6).

As a second benchmark test, we calculate the dynamic response of a half-space nonlinear granite model (Stevens et al., 2003) to an explosion of 20 tons yield in a 5-m spherical cavity, buried at a depth of 102 m, using the new 3D CRAM and the existing 2D CRAM. Figure 7 shows a comparison of seismograms at the free surface. The results show that the 3D CRAM calculations are also in excellent agreement with the existing 2D CRAM calculations, demonstrating that both codes, though implemented by different numerical methods, are capable of accurately computing nonlinear wave propagation in rocks due to explosions in a cavity.

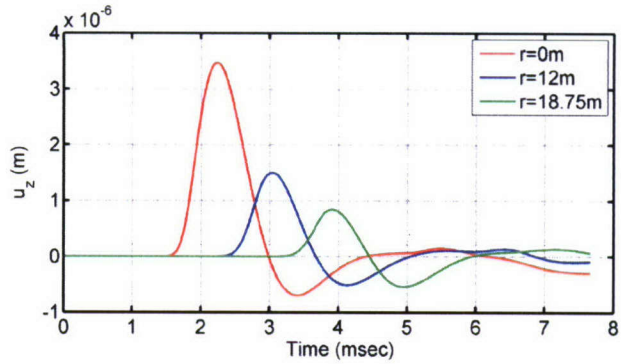

Figure 6. Dynamic response of a half-space to a pressure pulse applied to the wall of a buried spherical cavity. The figure shows the vertical component of displacement versus time. The results are consistent with the analytical solutions (Jiang et al., 1994).

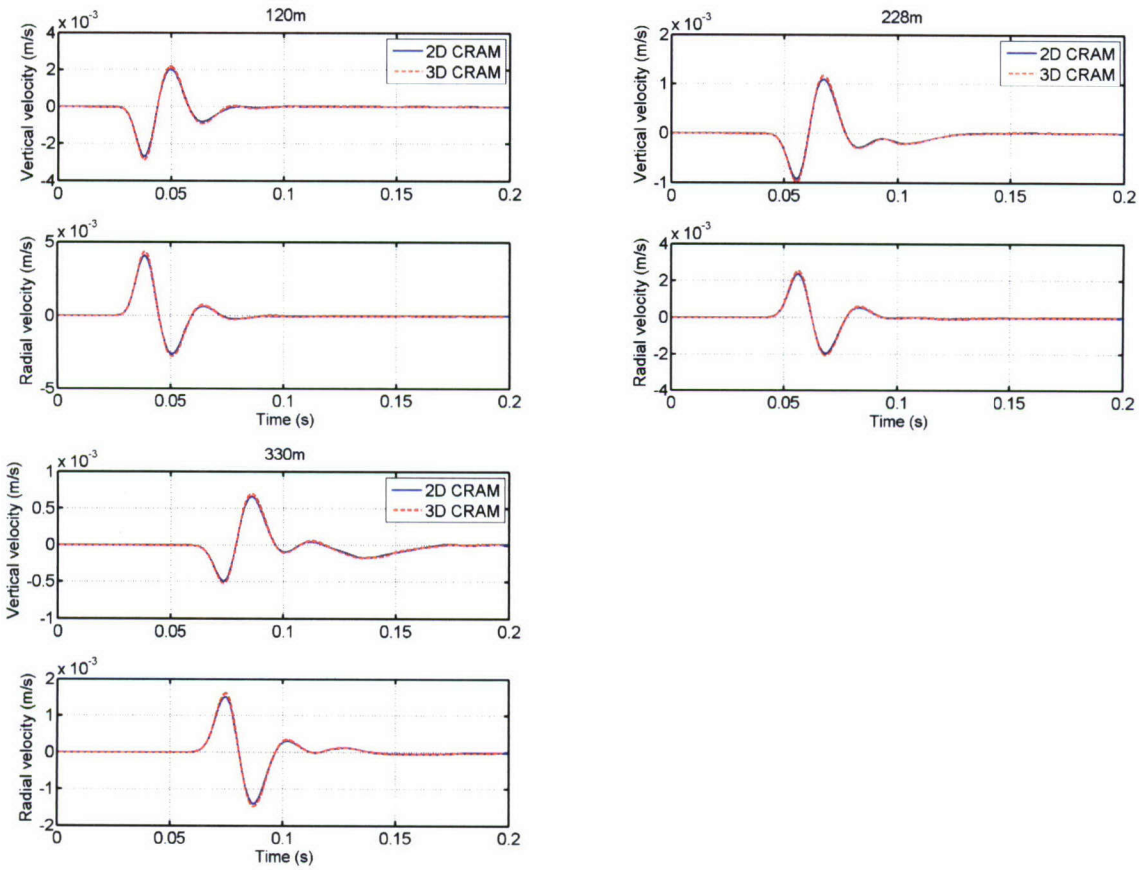

Figure 7. Comparisons of seismograms at three surface locations—120 m (top left), 228 m (top right), and 330 m (bottom). The top row shows the vertical component; the bottom shows radial. Blue lines are calculated with 2D CRAM; red lines are calculated with 3D CRAM.

Explosions in Rectangular and Spherical Cavities

To illustrate the effect of a nonspherical cavity in three dimensions, we compare the waveforms from detonating the same yield of 20 tons in a spherical cavity (red in Figure 8, left) and a cubic cavity (blue), both cavities having the same volume. The recordings at the 4 surface stations are compared in Figure 8 (right). Stations 1 and 3 are located at a distance of about 8-10 times the cavity size (about 3 times the nonlinear region size). Although the cavity volume is the same, the differences between the seismograms generated by the two cavity shapes are clearly visible on the three components. The explosion in the rectangular cavity is found to cause more nonlinear deformation around the cavity and to generate shear waves shown in the tangential direction.

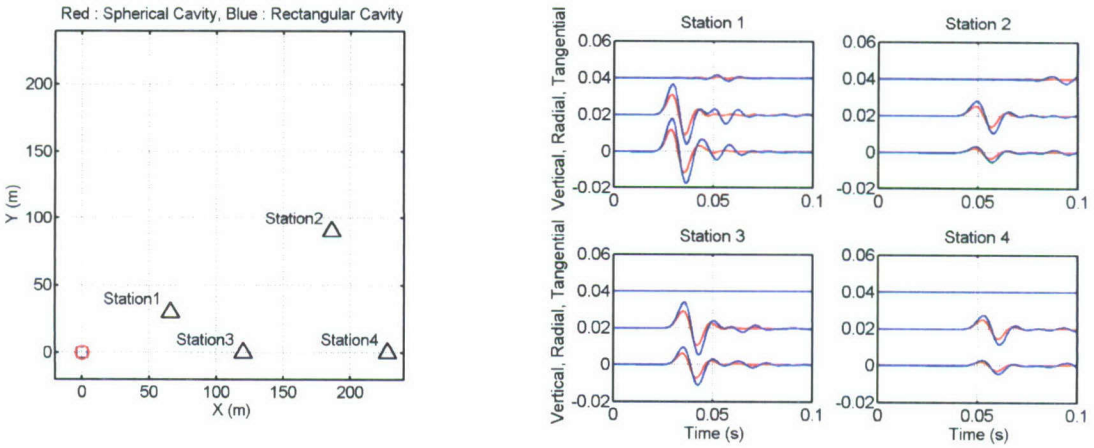

Figure 8. Map view of cavity and stations (left). Comparison of velocity seismograms at 4 locations (right). Red and blue lines correspond to spherical and rectangular cavities, respectively.

CONCLUSIONS AND RECOMMENDATIONS

We are in the early stages of a new project to understand 3D effects on seismic radiation from underground nuclear explosions. We have partially completed development of a 3D version of CRAM, the Lagrangian code we have used previously for performing axisymmetric calculations of underground explosions. We have also implemented a procedure for propagating the results of 3D source region calculations to regional and teleseismic distances using the representation theorem to couple source region calculations to a wavenumber integration code. Our plans are to complete implementation of the numerical methods and then perform 3D calculations to understand and model the effects of 3D source region heterogeneity and the seismic response to that heterogeneity.

REFERENCES

Aki, K. and P. G. Richards (1980). *Quantitative Seismology—Theory and Methods*. San Francisco: W. H. Freeman and Company.

Apsel, R. J. and J. E. Luco (1983). On the Green's functions for a layered half-space, Part II, *Bull. Seism. Soc. Am.* 73: 931–951.

Bache, T. C. and D. G. Harkrider (1976). The body waves due to a general seismic source in a layered earth model," *Bull. Seism. Soc. Am.* 66: 1805–1819.

Bache, T. C., S. M. Day, and H. J. Swanger (1982). Rayleigh wave synthetic seismograms from multi-dimensional simulations of underground explosions, *Bull. Seism. Soc. Am.* 72: 15–28.

Baker, G. E., J. L. Stevens, and H. Xu (2004). Lg group velocity: A depth discriminant revisited, *Bull. Seism. Soc. Am.* 94: 722–739.

Davis, C. G., W. E. Johnson, J. L. Stevens, N. Rimer, T. G. Barker, E. J. Halda, E. Bailey, and W. Proffer (1992). Seismic signals from asymmetric radiation-hydrodynamic calculations, Los Alamos National Laboratory report LA-12506-MS.

Day, S. M., J. T. Cherry, N. Rimer, and J. L. Stevens (1987). Nonlinear model of tectonic release from underground explosions, *Bull. Seism. Soc. Am.* 77: 996–1016.

Jiang, J., G. R. Baird and D. P. Blair (1994). Dynamic response of a half-space to a buried spherical source, *Geophys. J. Int.* 119: 753–765.

Kitov, I. O. (1997). Underground explosion seismic source function in various rock media as obtained from PNE local data, in upper mantle heterogeneities from active and passive seismology, K. Fuchs, Ed. Kulwer: 105–112.

Luco, J. E. and R. J. Apsel (1983). On the Green's functions for a layered half-space, Part I, *Bull. Seism. Soc. Am.* 73: 909–929.

Ma, S and P. Liu (2006). Modeling of the perfectly matched layer absorbing boundaries and intrinsic attenuation in explicit finite-element methods, *Bull. Seism. Soc. Am.* 96: 1779–1794.

Moczo, P., E. Bystricky, J. Kristek, J. M. Carcione, and M. Bouchon (1997). Hybrid modeling of P-SV seismic motion at inhomogeneous viscoelastic topographic structures, *Bull. Seism. Soc. Am.* 87: 1305–1323.

Murphy, J. R. and C. B. Archambeau (1986). Variability in explosion body-wave magnitudes: An analysis of the RULISON/GASBUGGY anomaly, *Bull. Seism. Soc. Am.* 76: 1087–1113.

Rimer, N., T. Barker, S. Rogers, J. Stevens, and D. Wilkins (1994). Simulation of seismic signals from partially coupled nuclear explosions in cylindrical tunnels, report DNA-TR-94-136, Defense Nuclear Agency, Alexandria, Va., August.

Stevens, J. L., S. Gibbons, N. Rimer, H. Xu, C. Lindholm, F. Ringdal, T. Kvaerna, and J. R. Murphy (2006). Analysis and simulation of chemical explosions in nonspherical cavities in granite, *J. Geophys. Res.* 111: B04306, doi:10.1029/2005JB003768.

Stevens, J. L., N. Rimer, H. Xu, G. E. Baker, and S. M. Day (2003). Near field and regional modeling of explosions at the Degelen test site, SAIC final report to DTRA, SAIC-02/2050, January.

Stevens, J. L., G. E. Baker, H. Xu, T. J. Bennett, N. Rimer, and S. M. Day (2004). The physical basis of Lg generation by explosion sources, SAIC final report submitted to the National Nuclear Security Administration under contract DE-FC03-02SF22676, December.

Stevens, J. L., T. G. Barker, S. M. Day, K. L. McLaughlin, N. Rimer, and B. Shkoller (1991). Simulation of teleseismic body waves, regional seismograms, and Rayleigh wave phase shifts using two-dimensional nonlinear models of explosion sources, AGU Geophysical Monograph 65: Explosion Source Phenomenology, S. Taylor, H. Patton, P. Richards, Eds., ISBN 0-87590-031-3, 239–252.

Wu, R. S., X. B. Xie, Z. Ge, and T. Lay (2004). Quantifying source excitation and path effects for high frequency regional waves, in *Proceedings of the 26th Annual Seismic Research Review: Trends in Nuclear Explosion Monitoring*, LA-UR-04-5801, Vol. 1, pp. 191–201.

Xie, X. B. and T. Lay (1994). The excitation of Lg waves by explosions: A finite difference investigation, *Bull. Seism. Soc. Am.* 84: 324–342.